

Space-borne Interferometers to Detect Thousands of Memory Signals Emitted by Stellar-mass Binary Black Holes

Shaoqi Hou,¹ Zhi-Chao Zhao,^{2,*} Zhoujian Cao,³ and Zong-Hong Zhu^{1,†}

¹*School of Physics and Technology, Wuhan University, Wuhan, Hubei 430072, China*

²*Department of Applied Physics, College of Science, China Agricultural University, Qinghua East Road, Beijing 100083, People's Republic of China*

³*Department of Astronomy, Beijing Normal University, Beijing 100875, China*

(Dated: November 28, 2024)

The gravitational memory effect manifests the nonlinearity of the gravitation, reflects the degenerate gravitational vacua, and indicates the types of the asymptotic symmetries. However, by the received wisdom, it would be challenging to detect it. In this Letter, we envisioned employing the space-borne interferometer, especially DECIGO, to detect memory signals generated by the stellar-mass binary black hole (BBHs) systems, the conventional targets of the ground-based detectors. We estimated that during its 5 years' observation, DECIGO could detect nearly 2,258 loud enough memory signals. Among them, 102 have signal-to-noise ratios greater than 8. Our prediction was obtained with the BBH population model constrained by the recent gravitational wave observations in GWTC-3. The Power Law + Peak mass model and the DEFAULT spin model were employed, and the merger rate was chosen to be proportional to the Madau-Dickinson formation rate. In the analysis, the impact of the orbital eccentricity was also considered. The high rate is due to the sufficiently strong memory signal right at the bandwidth of DECIGO, and also because of the humongous number of the surely existing stellar-mass BBHs. The substantial, and yet conservative, number of detections enables to leverage statistical approaches to harness the memory effect for fundamental physics and astrophysics.

I. INTRODUCTION

The memory effect is a direct prediction of general relativity resulting from its nonlinearity [1–4]. It causes a permanent change in the spacetime metric, resulting in the arms of interferometers being stretched or contracted permanently. It is closely connected to the Bondi-Metzner-Sachs (BMS) symmetries [5] of isolated systems [6, 7]. As a form of BMS symmetry, supertranslations transform degenerate gravitational vacuum states into one another, manifesting as the memory effect [8–10]. The null energy flux, which is the Noether charge conjugate to supertranslation, serves as the source of the (nonlinear) memory effect [6, 10]. Spin and center-of-mass (CM) memories were recently discovered [11–13]. To account for these effects, the BMS group must be appropriately generalized [14–18]. To differentiate them, the earlier memory effect is specifically referred to as displacement memory. Generally, displacement memory is the strongest, while CM memory is the weakest [12, 13]. In this Letter, we will focus on displacement memory, referred to simply as *the* memory effect unless otherwise specified.

There are several intriguing applications of memory effects. For instance, the memory effect can be used to test the consistency between different waveform models [19]. It may also help distinguish neutron star-black hole (NS-BH) mergers from binary black hole (BBH) mergers [20],

and by considering matter effects, it could differentiate binary neutron star (BNS) mergers from NS-BH mergers as well [21]. Incorporating nonlinear memory waveforms in parameter estimation might break the degeneracy between the inclination angle ι and the luminosity distance D_L , especially for equal-mass, non-precessing binaries [22]. Additionally, it has been suggested that observing specific memory effects could reveal the corresponding asymptotic symmetries [23]. Studies on modified gravity theories proposed using the memory effect to probe the nature of gravity [24–31]. Furthermore, since the memory effect does not manifest in odd spacetime dimensions, detecting it would rule out such higher-dimensional models [32, 33].

However, due to the signal's weakness, no memory effect has been detected by interferometers [34–40] or pulsar timing arrays [41]. Recently, the North American Nanohertz Observatory for Gravitational Waves (NANOGrav) set a median upper limit of approximately 3.3×10^{-14} on the strain of the memory effect [41]. To date, studies have predicted that detecting the memory effect is challenging. For example, networks of the LVK detectors and LIGO India may accumulate sufficient signal-to-noise ratios (SNRs), at least 3, for the memory effect after 3 to 5 years of observing hundreds or thousands of stellar-mass BBH merger events [36, 42]. A network of 2 or 3 Cosmic Explorers (CEs) could detect memory effects from individual loud events, with a yearly detection rate of 4 to 7 [42]. TianQin is expected to detect around 0.5 to 2 memory signals (SNRs ≥ 3) during its 5-year operation [43]. LISA, on the other hand, is predicted to observe tens to hundreds of memory signals (SNRs ≥ 1) from massive BBHs over its 4-year operation.

* zhaozc@cau.edu.cn

† zhuzh@whu.edu.cn

If the SNR threshold is set to 5, a few to tens of signals may be observable [44, 45].

Although these predictions hold promise for detecting this interesting phenomenon, the relatively low rates may limit the practical applications of memory effects. Faced with such a situation, one shall realize that in the previous works [36, 42–45], people conventionally considered the memory effect produced by the very binaries chirping at the bandwidths of the respective interferometers. However, the memory signal may actually be strong at relatively lower frequency ranges. So in this Letter, we instead proposed to use the space-borne interferometer to detect the memory effect generated by stellar-mass BBHs, which are abundant and usually thought to be the targets of the ground-based interferometers. In particular, the DECihertz laser Interferometer Gravitational wave Observatory (DECIGO) [46–48] is well suited for this purpose [49]. We will show that the memory signals produced by these sources are sufficiently loud for DECIGO, due to its low frequency nature, and so the detect rates are substantially high. Moreover, the stellar-mass BBHs have been confirmed to exist by the observations of the LVK collaboration, allowing for more reliable estimates of their coalescence rates.

II. MEMORY WAVEFORM

The memory effect h_D can be effectively calculated using the flux-balance laws [6, 50] in the Bondi-Sachs coordinates (u, r, θ, ϕ) [51, 52],

$$h_D = r \sum_{\widetilde{\ell}} \widetilde{-2Y_{\ell m}} \sqrt{\frac{(\ell-2)!}{(\ell+2)!}} \mathcal{C}_{\ell}(-2, \ell_1, m_1; 2, \ell_2, -m_2) \times (-1)^{m_2} \int_{u_0}^u \dot{h}_{\ell_1 m_1} \dot{\bar{h}}_{\ell_2 m_2} du'. \quad (1)$$

Here, in this formula, $_{-2}Y_{\ell m}(\theta, \phi)$ is the spin-weighted spherical harmonics, $h_{\ell m}$ is the spherical mode of the complex strain $h = h_+ - ih_{\times} = \sum_{\ell m} _{-2}Y_{\ell m} h_{\ell m}$, dot means ∂_u , bar means to take the complex conjugate, and the sum $\sum_{\widetilde{\ell}}$ runs over (ℓ, m) , (ℓ_1, m_1) and (ℓ_2, m_2) . One also defines [12]

$$\mathcal{C}_{\ell}(s_1, \ell_1, m_1; s_2, \ell_2, m_2) \equiv \int d^2\theta \sin\theta ({}_{s_1}Y_{\ell_1 m_1}) ({}_{s_2}Y_{\ell_2 m_2}) ({}_s\bar{Y}_{\ell m}), \quad (2)$$

which vanishes unless $s = s_1 + s_2$, $m = m_1 + m_2$, and $\max\{|\ell_1 - \ell_2|, |m_1 + m_2|, |s_1 + s_2|\} \leq \ell \leq \ell_1 + \ell_2$. In Eq. (1), one ignores the so-called linear memory effect, which is smaller than the nonlinear one given by this expression [50]. For the details of the derivation of this result, please refer to Appendix A. According to Refs. [53–56], the memory waveform is mainly given by the terms

with $\ell = 2, 4$ and $m = 0$ in Eq. (1), i.e.,

$$h_D \approx \frac{(17 + \cos^2 \iota) \sin^2 \iota}{384\pi} r \times \int_{u_0}^u du' \int d^2\theta \sin\theta (\dot{h}_+^2 + \dot{h}_{\times}^2),$$

where ι is the inclination angle. This results in the *minimal-waveform* model [55], which has already been implemented in the **GWMemory** package [57].

The memory waveform h_D increases monotonically over time, as illustrated in Fig. 1, which shows h_D generated by a stellar-mass binary system like GW150914, alongside the corresponding oscillatory mode h_+^{osc} , dominated by the quadruple radiation $h_{2, \pm 2}$. The frequency-

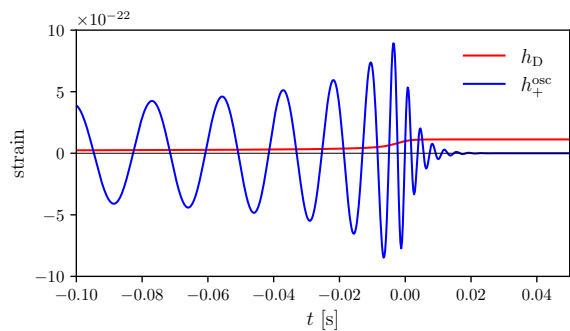


FIG. 1. Time-domain waveforms produced by PyCBC from a GW150914-like binary system with IMRPhenomD [58, 59]. The blue curve represents the $+$ -polarization of the oscillatory mode h_+^{osc} , while the red curve illustrates the memory waveform h_D . The inclination angle is set to $\iota = \pi/2$ to maximize the magnitude of the memory effect for demonstration purposes.

domain memory waveform can be obtained by formally replacing the integral in Eq. (1) with

$$-i2\pi f^{-1} \int f'(f' - f) \tilde{h}_{\ell_1 m_1}(f') \tilde{h}_{\ell_2 m_2}^*(f' - f) df', \quad (3)$$

where $\tilde{h}_{\ell m}(f)$ is the Fourier transform and $\tilde{h}_{\ell m}^*(f)$ is its complex conjugate. In Fig. 5, the Fourier-transformed waveforms \tilde{h}_D and \tilde{h}_+^{osc} are shown. The noise power spectral density (PSD) of DECIGO is also plotted. In calculating this PSD, we have accounted for the contamination from foreground galactic and extra-galactic compact binaries, as well as neutron stars [60–65]. For a detailed explanation of the PSD construction and the computation of the SNR, please refer to Appendix B. Clearly, the red curve for the memory effect is well above the PSD of DECIGO at the certain frequency range. It turned out that the SNR of \tilde{h}_D is ~ 114 . Therefore, even though a stellar-mass BBH chirps around $O(100)$ Hz, its memory signal could still be detected by DECIGO.

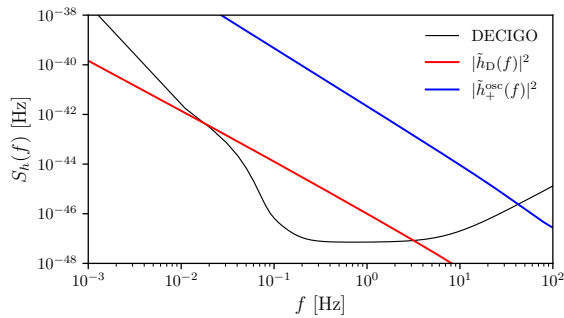


FIG. 2. The frequency-domain memory waveform \tilde{h}_D and the corresponding oscillatory component \tilde{h}_+^{osc} are plotted. The black curve represents the noise power spectrum of DECIGO. The squared moduli of \tilde{h}_D and \tilde{h}_+^{osc} are shown for comparison with the black curve.

III. SIMULATIONS AND RESULTS

In our simulation, we generated BBHs with randomly assigned right ascension (RA), declination (DEC), inclination angle ι , and coalescence phase ϕ . The binary components follow quasi-circular orbits, with their spins aligned with the orbital angular momentum. Their masses, spins, and merger rates were sampled from some relevant population synthesis models. Specifically, we used the Power Law + Peak mass model and the DE-FAULT spin model to characterize the mass and spin distributions, with the results of Ref. [66] serving as fiducial parameters. For the evolution of the merger rate with redshift, given that the BBH detection horizon is smaller than the expected peak redshift z_p , where the merger rate is maximized, the LVK detectors were unable to effectively model the merger rate at high redshifts. Therefore, we adopted the LVK-constrained local merger rate R_0 , which falls within the range of $17.9 \text{ Gpc}^{-3} \text{ yr}^{-1}$ to $44 \text{ Gpc}^{-3} \text{ yr}^{-1}$ at $z = 0.2$ at the 90% credible interval (C.L.). We further assumed that the merger rate is proportional to the Madau–Dickinson star formation rate model [67], which is consistent with the low-redshift merger rate inferred by LVK [66]. The distributions of chirp mass \mathcal{M} , mass ratio $q = m_1/m_2$, and redshift z are displayed in Fig. 6. As shown, most of the sampled BBH systems have small chirp masses, with $\mathcal{M} \sim 8M_\odot$ and $q \sim 1$, while their redshifts range from 1 to 4.

Using the sampled BBHs, we employed GWMemory [68] to generate their memory waveforms, assuming the oscillatory parts last for 5×10^3 seconds. To claim the detection of a specific GW signal, it is generally required that $\rho \geq 8$ [69, 70]. However, different thresholds, such as $\rho \geq 10$ and $\rho \geq 5$, have also been employed in some cases [71–74]. For memory signals, a fourth threshold of $\rho \geq 3$ is advocated in Refs. [34, 42, 75]. So, Table II lists the numbers of detectable memory signals during DECIGO’s 5-year observation period, meeting the different SNR thresholds. It shows that up to 2,258 mem-

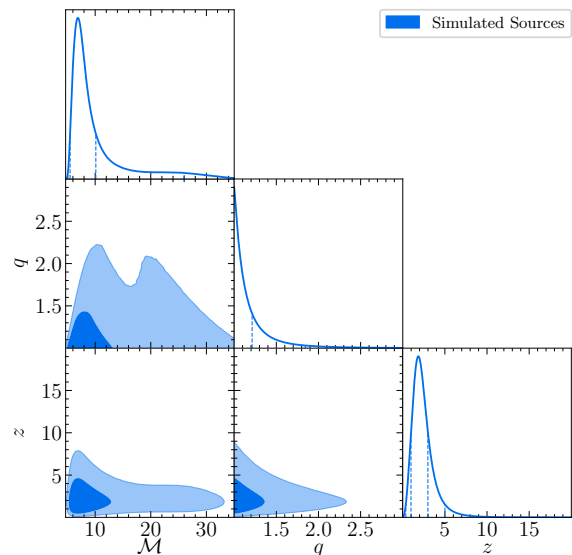


FIG. 3. The distributions of the source-frame chirp mass \mathcal{M} , mass ratio $q = m_1/m_2$, and redshift z , sampled from binary black hole population model obtained by LVK using GWTC-3.

SNR Thresholds	10	8	5	3
Event Numbers	~ 54	~ 102	~ 499	~ 2258

TABLE I. The numbers of memory signals with sufficiently high SNRs that might be detected by DECIGO during its 5-year operation, assuming $R_0 = 17.9 \text{ Gpc}^{-3} \text{ yr}^{-1}$, the 90% C.L. lower limit. Note that if the upper limit were used, the event counts would be increased by a factor of 1.5.

ory signals with SNRs > 3 could be observed by DECIGO. We also found out that among the 54 loudest events (the second column), 8 of them have SNRs, accumulated *solely* in the inspiral stage, greater than 3 [76]. Note that $R_0 = 17.9 \text{ Gpc}^{-3} \text{ yr}^{-1}$ (90% C.L. lower limit) was chosen in this simulation. If $R_0 = 44 \text{ Gpc}^{-3} \text{ yr}^{-1}$ (the upper limit) were used instead, the resulting rates would be increased by a factor of 1.5.

Figure 7 shows the distributions of \mathcal{M} , q , and z for events with memory SNRs of at least 3 or 8. As shown, the observable memory signals for DECIGO would be mainly produced by BBHs with $\mathcal{M} \sim 30M_\odot$. A large fraction of these systems have $q \sim 1$. If the detection threshold is set to 3, these sources are dominated by BBHs with $0.25 \lesssim z \lesssim 1.5$. Naturally, if the threshold is 8, only lower redshift ($\lesssim 0.5$) sources produce sufficiently strong memory signals. The redshift distributions suggest the robustness of our predictions, as the merger rate provided by the LVK is reliable for $z \lesssim 1.5$. In Appendix C, similar estimations were presented based on the different population models in Ref. [77].

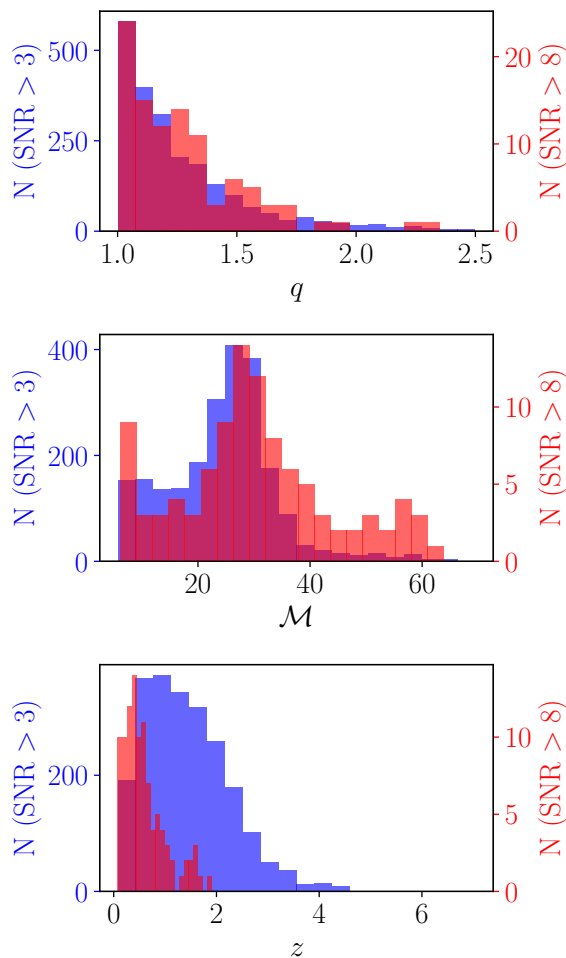


FIG. 4. The distributions of \mathcal{M} , q , and z for events with memory SNRs of at least 3 or 8. The left vertical axis corresponds to memory SNR > 3 , with a different scale from the right axis, which is for memory SNR > 8 .

IV. THE IMPACTS OF ECCENTRICITIES

Since the LVK collaboration constrained the population model of BBHs assuming the quasi-circular orbits [66], the simulated merger events in this Letter have the vanishing eccentricity. However, the orbit is generally elliptical owing to various astrophysical mechanisms [78], and the eccentricity might be large in the bandwidth of DECIGO. The eccentricity certainly affects the waveform, but we found out that the SNR changes little.

To investigate the influence of the eccentricity on the SNR, we used SEOBNRE [79, 80] to simulate $h_{2,\pm 2}$, assuming $m_1 = m_2 = 30M_\odot$, $D_L = 400$ Mpc, $\iota = \pi/2$ and vanishing spins. One has to set the eccentricity at 10 Hz following the usage of SEOBNRE, although it is capable of calculating the waveform starting at decihertz. The eccentricities were chosen to be 0.3, 0.2, 0.1, 0.05, 0.01, and 0 at 10 Hz, which correspond to 0.99, 0.98, 0.92, 0.72, 0.15, and 0, respectively, about 5×10^3 seconds before the

merger. Then with Eq. (1) to get h_D , one found out that the SNRs are $84 \sim 85$, showing insignificant impacts of eccentricities on SNRs. Since we estimated the memory rates based on the SNR, our results are still robust.

V. DISCUSSIONS AND CONCLUSION

According to Table II, DECIGO will detect approximately 452 BBH merger events per year with memory SNRs > 3 . Such a substantial number surpasses all previous predictions for any detector [36, 42–45], highlighting the exceptional capability of using the space-borne interferometer to detect an extensive population of stellar-mass BBHs, whose existence has been confirmed by the LVK collaboration. By concentrating on these sources, our work significantly distinguishes itself from studies involving (super)massive BBHs for LISA and TianQin [43–45] — especially considering that the final parsec problem remains unresolved [81]. Additionally, due to the limited sensitivities at $O(10)$ Hz and below, the LVK detectors might miss some BBH merger events, which could be captured by DECIGO. Therefore, we might provide the lower bounds.

The detection of numerous memory signals offers new opportunities for fundamental physics and astrophysics through statistical methods. For example, global waveform fitting can help examine the sky distribution of memory events, useful for identifying anisotropies in memory SNR. Also, exploring correlations between memory strength and other parameters, such as mass and spin, can provide insights into nonlinear gravitational dynamics. The asymptotic symmetries might be better pinned down by analyzing these memory signals statistically [23]. Moreover, different waveform models can be crosschecked based on the flux-balance laws [19], also using certain statistical methods.

Since a large fraction of memory signals come from BBHs with $q \sim 1$ and no precession, the degeneracy between ι and D_L can thus be broken, which cannot be achieved with the higher multiple modes for such systems [22]. This allows for a more accurate determination of D_L , and if z can be obtained, such BBHs would make excellent dark sirens [82, 83], which are essential for cosmological studies, including the measurement of the Hubble constant. Although the detection rates for BNS and NS-BH events were not calculated, they are also expected to be quite high, compared to other interferometers. Memory signals could help distinguish these systems, as suggested in Refs. [20, 21], improving the estimation of merger rates for different binary types and enhancing our understanding of their formation.

As mentioned, 8 events' memory SNRs, accumulated *solely* in the inspiral phase, are > 3 . These events are crucial for testing the memory effect predicted in modified theories of gravity, as nearly all waveforms in these theories have been, or could be, calculated only for the inspiral stage [24, 28, 30, 84–86]. Since dipole radia-

tion generally exists in these theories and increases more rapidly at lower frequencies [28, 87, 88], its contribution to the memory waveform may be more easily detected by DECIGO. Similarly, certain higher-dimensional models could be better constrained or even ruled out.

While next-generation ground-based interferometers like Einstein Telescope (ET) and CE also focus on stellar-mass BBHs, their performance at low frequencies is not as advantageous as that of DECIGO. However, ET and CE could join with DECIGO if they operate concurrently. It would enhance the scientific returns of GW observations, allowing for cross-validation of detections and improved parameter estimations. We leave the detailed exploration of such synergistic observations for future work.

One thus expects that the high detection rates provided by DECIGO would eventually make the study of the memory effect to be more practical, ceasing to be of merely theoretical interest.

ACKNOWLEDGMENTS

Z.C.Z would like to thank Xiaolin Liu for help with SEOBNRE code. This work was supported by the National Natural Science Foundation of China under grant Nos. 11633001 and 11920101003, the Key Program of the National Natural Science Foundation of China under grant No. 12433001, and the Strategic Priority Research Program of the Chinese Academy of Sciences, grant No. XDB23000000. S. H. was supported by the National Natural Science Foundation of China under Grant No. 12205222. Z.C.Z. was supported by the National Key Research and Development Program of China Grant No. 2021YFC2203001. This work was also supported by High-performance Computing Platform of China Agricultural University.

Appendix A: Memory waveform

In the Bondi-Sachs formalism, after solving the vacuum Einstein's equation, one writes the metric in the coordinates (u, r, θ, θ) in the following way [6, 50, 86],

$$\begin{aligned} ds^2 = & -du^2 - 2dudr + r^2\gamma_{AB}d\theta^A d\theta^B \\ & + \frac{2m}{r}du^2 + \mathcal{D}^B c_{AB}dud\theta^A + rc_{AB}d\theta^A d\theta^B \quad (\text{A1}) \\ & + \dots, \end{aligned}$$

where m is the Bondi mass aspect, γ_{AB} is the round metric on a unit 2-sphere, c_{AB} is the shear tensor, and \mathcal{D}_A is the covariant derivative compatible with γ_{AB} . The indices $A, B (= 1, 2)$ are lowered and raised by γ_{AB} and its inverse γ^{AB} , respectively. The first line is the Minkowski metric, and the following lines represent the leading order contributions to the metric for a generic asymptotically flat spacetime. The dots stand for higher order terms in

$1/r$ that are irrelevant to the following discussion. From this metric, one knows that r is null, and the GW propagates in this direction at $r \rightarrow +\infty$. u is the retarded time, measuring the phase of the GW.

The test particles, such as the mirrors in the interferometer, are located at a large distance r , roughly taken to be $+\infty$. Their 4-velocities are approximately ∂_u . Including this vector field, one can set up an pseudo-orthogonal tetrad basis, given by [86],

$$e_{\hat{0}} = \partial_u + \dots, \quad (\text{A2})$$

$$e_{\hat{r}} = \partial_u - \partial_r + \dots, \quad (\text{A3})$$

$$e_{\hat{1}} = \frac{1}{r}\partial_{\theta^1} + \dots, \quad (\text{A4})$$

$$e_{\hat{2}} = \frac{1}{r \sin \theta_1}\partial_{\theta^2} + \dots, \quad (\text{A5})$$

adapted to the Bondi-Sachs coordinates. The hatted capital Latin indices will be raised or lowered by $\gamma^{\hat{A}\hat{B}} (= \delta^{\hat{A}\hat{B}})$ and $\gamma_{\hat{A}\hat{B}}$, respectively. Let the deviation vector between two test particles be given by

$$\vec{S} = S^{\hat{A}}e_{\hat{A}}, \quad (\text{A6})$$

which satisfies the geodesic deviation equation [89],

$$\ddot{S}^{\hat{A}} = -R_{\hat{0}\hat{B}\hat{0}}^{\hat{A}}S^{\hat{B}}. \quad (\text{A7})$$

Substituting the metric (A1) into the Riemann tensor, one has

$$R_{\hat{0}\hat{A}\hat{0}\hat{B}} = -\frac{1}{2r}\ddot{c}_{\hat{A}\hat{B}} + \dots. \quad (\text{A8})$$

Therefore, a generic time-dependent shear c_{AB} represents the GW. Let us assume that the GW exists from u_0 to u_f , and the initial deviation vector is $S_0^{\hat{A}}$. Integrating Eq. (A8) twice, one obtains [29]

$$\Delta S^{\hat{A}} = \frac{\Delta c_{\hat{A}\hat{B}}}{2r}S_0^{\hat{B}}, \quad (\text{A9})$$

with higher order terms ignored. In this equation, $\Delta u = u_f - u_0$, and $\Delta c_{\hat{A}\hat{B}} = c_{\hat{A}\hat{B}}(u_f) - c_{\hat{A}\hat{B}}(u_0)$. If $\Delta S^{\hat{A}} \neq 0$, one claims the existence of the memory effect. When this happens, $\Delta c_{AB} \neq 0$.

As c_{AB} is a traceless rank-2 tensor on the 2-sphere, one decomposes it in the following way [6],

$$c_{AB} = \left(\mathcal{D}_A \mathcal{D}_B - \frac{\gamma_{AB}}{2} \mathcal{D}^2 \right) \Phi + \epsilon_{C(A} \mathcal{D}_{B)} \mathcal{D}^C \Psi, \quad (\text{A10})$$

where ϵ_{AB} is the volume element of the 2-sphere, and $\mathcal{D}^2 = \mathcal{D}_A \mathcal{D}^A$. The scalar functions Φ and Ψ determine the electric and the magnetic components of c_{AB} , respectively. Before the arrival of the GW, or after its disappearance, Φ and Ψ are both time independent. It is also possible to find a special frame, namely, the canonical Bondi frame, in which $\Psi = 0$, according to Ref. [6]. The memory effect is also referred to

$$\Delta \Phi = \Phi(u_f) - \Phi(u_0), \quad (\text{A11})$$

in the canonical Bondi frame.

Einstein's equation can be used to calculate the displacement memory effects. That is, one uses the following evolution equation for m [6],

$$\dot{m} = \frac{1}{4} \mathcal{D}_A \mathcal{D}_B N^{AB} - \frac{1}{8} N_{AB} N^{AB}, \quad (\text{A12})$$

where the overhead dot means ∂_u , and $N_{AB} \equiv \dot{c}_{AB}$ is the news tensor. Integrating this equation and rearranging, one gets

$$\mathcal{D}_A \mathcal{D}_B \Delta c^{AB} = 4\Delta m + \frac{1}{2} \int_{u_0}^{u_f} du N_{AB} N^{AB}. \quad (\text{A13})$$

On the right-hand side, the first term gives the linear memory, while the second term is the nonlinear memory, which is sourced by the energy flux of the GW [90]. Usually, the linear memory is smaller than the nonlinear one [50], and has nothing to do with the nonlinearity of GR, so it will be neglected in this work. In terms of $\Delta\Phi$ and ignoring the ordinary memory effect, one can write

$$\mathcal{D}^2 (\mathcal{D}^2 + 2) \Delta\Phi = \int_{u_0}^{u_f} du N_{AB} N^{AB}. \quad (\text{A14})$$

Note that the upper limit of the integration is u_f , the time when the GW disappears, so the above equation gives the total displacement memory effect. The waveform of the displacement memory effect is given by the same equation with the upper limit being an arbitrary time $u (> u_0)$.

To reexpress Eq. (A14), it is convenient to first set up complex dyads for the unit round metric γ_{AB} , given by [50],

$$\gamma_A = -(1, i \sin \theta), \quad \bar{\gamma}_A = -(1, -i \sin \theta). \quad (\text{A15})$$

With these, one has $\gamma_{AB} = (\gamma_A \bar{\gamma}_B + \bar{\gamma}_A \gamma_B)/2$. It is conventional to introduce the complex waveform [50]

$$h \equiv \frac{1}{2r} \bar{\gamma}^A \bar{\gamma}^B c_{AB} = \sum_{\ell=2}^{\infty} \sum_{m=-\ell}^{\ell} {}_{-2}Y_{\ell m} h_{\ell m}, \quad (\text{A16})$$

which has been expanded using the spin-weighted spherical harmonics ${}_{-2}Y_{\ell m}(\theta^A)$. The expansion coefficients $h_{\ell m}$ are the spherical modes. The dominating modes are h_{22} and $h_{2,-2}$, i.e., the quadruple moments. They are the oscillatory modes, and are implemented in all of the waveform templates. The higher spherical modes might be implemented in some of the waveform templates, such as IMRPhenomXPHM [91]. In terms of h , the shear tensor is

$$c_{AB} = \frac{r}{2} (\gamma_A \gamma_B h + \bar{\gamma}_A \bar{\gamma}_B \bar{h}), \quad (\text{A17})$$

with \bar{h} the complex conjugate of h .

As discussed previously, Eq. (A14) determines the null displacement memory effect, $\Delta\Phi$. To compute it, first, decompose $\Delta\Phi$ such that

$$\Delta\Phi = \sum_{\ell m} \Delta\Phi_{\ell m} Y_{\ell m}, \quad (\text{A18})$$

and then, substitute it into Eq. (A14), together with Eq. (A17), resulting in

$$\begin{aligned} \Delta\Phi_{\ell m} = & 2r^2 \frac{(\ell-2)!}{(\ell+2)!} \widetilde{\sum} \mathcal{C}_{\ell}(-2, \ell_1, m_1; 2, \ell_2, -m_2) \\ & \times (-1)^{m_2} \int_{u_0}^u \dot{h}_{\ell_1 m_1} \dot{\bar{h}}_{\ell_2 m_2} du', \end{aligned} \quad (\text{A19})$$

where the sum $\widetilde{\sum}$ is over ℓ_1, m_1 and ℓ_2, m_2 . In this expression, one defines a symbol

$$\begin{aligned} \mathcal{C}_{\ell}(s_1, \ell_1, m_1; s_2, \ell_2, m_2) \\ \equiv \int d^2\theta \sqrt{\gamma}(s_1 Y_{\ell_1 m_1})(s_2 Y_{\ell_2 m_2})(s \bar{Y}_{\ell m}), \end{aligned} \quad (\text{A20})$$

which vanishes unless $s = s_1 + s_2$, $m = m_1 + m_2$, and $\max\{|\ell_1 - \ell_2|, |m_1 + m_2|, |s_1 + s_2|\} \leq \ell \leq \ell_1 + \ell_2$. $\Delta\Phi_{\ell m}$ are directly related to the complex waveform h in the following way,

$$\begin{aligned} h_D = & \frac{1}{2} \gamma^A \gamma^B \Delta c_{AB} \\ = & \frac{1}{2} \gamma^A \gamma^B \left(\mathcal{D}_A \mathcal{D}_B - \frac{\gamma_{AB}}{2} \mathcal{D}^2 \right) \Delta\Phi \\ = & \sum_{\ell=2}^{\infty} \sum_{m=-\ell}^{\ell} {}_{-2}Y_{\ell m} \Delta h_{\ell m}, \end{aligned} \quad (\text{A21})$$

where Eq. (A10) has been used, ignoring the magnetic component (Ψ), relevant to the spin memory. Therefore, after some mathematical manipulation using the $\bar{\partial}$ -calculus [92], one has [22, 50]

$$\Delta h_{\ell m} = \frac{1}{2r} \sqrt{\frac{(\ell+2)!}{(\ell-2)!}} \Delta\Phi_{\ell m}. \quad (\text{A22})$$

Although not explicit, $\ell \geq 2$ in this equation. This equation gives the total change in the electric component of the GW for any mode (ℓ, m) . Combining Eqs. (A19), (A21) and (A22), one obtains Eq. (1) in the Main text.

To get the waveform in the frequency domain, it is sufficient to compute the Fourier transform of the integral in Eq. (A19). So one gets

$$\begin{aligned} \Delta\tilde{\Phi}_{\ell m}(f) = & 2r^2 \frac{(\ell-2)!}{(\ell+2)!} \widetilde{\sum} \mathcal{C}_{\ell}(-2, \ell_1, m_1; 2, \ell_2, -m_2) \\ & \times (-1)^{m_2} \frac{2\pi}{if} \int f'(f' - f) \tilde{h}_{\ell_1 m_1}(f') \tilde{h}_{\ell_2 m_2}^*(f' - f) df', \end{aligned} \quad (\text{A23})$$

where the Fourier transformation is defined to be

$$\tilde{h}_{\ell m}(f) = \int_{-\infty}^{+\infty} h_{\ell m}(u) e^{-i2\pi f u} du. \quad (\text{A24})$$

Note the existence of f in the denominator of Eq. (A23). This is one of key characteristics of the frequency domain memory waveform. Equation (A23) allows one to compute the Fourier domain memory waveform produced in the inspiral phase by substituting the corresponding oscillatory waveform in the frequency domain.

Appendix B: The noise power spectrum density

DECIGO is a gravitational wave (GW) detector composed of four copies of constellations of three drag-free spacecrafts [46–48]. In each constellation, the spacecrafts are separated from each other by about 1,000 km, and they orbit around the Sun with a period of 1 yr. Each constellation can be equivalently viewed as two uncorrelated, L-shaped detectors rotated by 45°. The one-sided noise power spectrum of an L-shaped interferometer can be written as [63, 64]:

$$\begin{aligned} \bar{S}_n(f) &= 7.05 \times 10^{-48} \left[1 + \left(\frac{f}{f_p} \right)^2 \right] \\ &+ 4.8 \times 10^{-51} \left(\frac{1 \text{ Hz}}{f} \right)^4 \left[1 + \left(\frac{f}{f_p} \right)^2 \right]^{-1} \\ &+ 5.53 \times 10^{-52} \left(\frac{1 \text{ Hz}}{f} \right)^4 \text{ Hz}^{-1}, \end{aligned} \quad (\text{B1})$$

with $f_p = 7.36$ Hz. The galactic and the extra-galactic compact binaries in the foreground would produce GWs that contaminate the sensitivity. The effective noise power spectra due to these GWs are given by [60, 61],

$$\begin{aligned} S_n^g(f) &= 2.1 \times 10^{-45} \left(\frac{1 \text{ Hz}}{f} \right)^{7/3} \text{ Hz}^{-1}, \\ S_n^{\text{eg}}(f) &= 4.2 \times 10^{-47} \left(\frac{1 \text{ Hz}}{f} \right)^{7/3} \text{ Hz}^{-1}, \end{aligned} \quad (\text{B2})$$

respectively. These spectra should be further multiplied by a factor corresponding to the high-frequency cutoff,

$$F(f) = \exp \left[-2 \left(\frac{f}{0.05 \text{ Hz}} \right)^2 \right].$$

The noise from neutron stars (NS) should also be considered. However, following [62], we assume most (99%) of them can be removed by foreground subtraction. Then, the noise is

$$\begin{aligned} S_n'^{\text{NS}}(f) &= 0.01 \times S_n^{\text{NS}}(f) \\ &= 1.3 \times 10^{-48} \left(\frac{1 \text{ Hz}}{f} \right)^{7/3} \text{ Hz}^{-1}. \end{aligned} \quad (\text{B3})$$

The overall noise power is

$$\begin{aligned} S_n(f) &= S_n^{\text{eg}}(f)F(f) + S_n'^{\text{NS}}(f) + \min \left\{ \bar{S}_n(f) \right. \\ &\left. + S_n^g(f)F(f), \frac{\bar{S}_n(f)}{\exp(-\kappa T_{\text{obs}}^{-1} \frac{dN}{df})} \right\}. \end{aligned} \quad (\text{B4})$$

In this expression, the symbol min implies to take the smaller argument. T_{obs} is the observation time, which

is set to 5 yrs. dN/df is the number density of white dwarfs in the galaxy per unit frequency,

$$\frac{dN}{df} = 2 \times 10^{-3} \left(\frac{1 \text{ Hz}}{f} \right)^{11/3} \text{ Hz}^{-1}.$$

And finally, the factor appearing in the exponential function is $\kappa = 4.5$ [65]. The noise spectrum Eq. (B4) is reproduced in Fig. 5, together with the squared moduli of a GW150914-like memory signal \tilde{h}_D and its oscillatory counterpart \tilde{h}_+^{osc} .

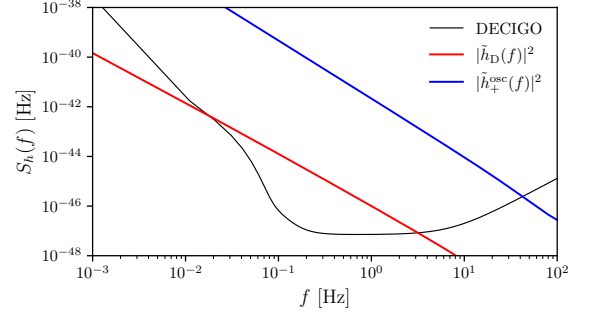


FIG. 5. The frequency-domain memory waveform \tilde{h}_D together with the corresponding oscillatory component \tilde{h}_+^{osc} are plotted. The black curve is the noise power spectrum of DECIGO.

With Eq. (B4), one can calculate the signal-to-noise ratio for the memory waveform with

$$\rho^2 = 4\sqrt{8} \int_0^\infty \frac{|\tilde{h}_D(f)|^2 K^2(f)}{S_n(f)} df. \quad (\text{B5})$$

Here, the factor $K(f)$ is given by [93],

$$K(f) = \frac{3}{10} \frac{1}{1 + (f/f_*)^2 / [1.85 - 0.58 \cos(2f/f_*)]}, \quad (\text{B6})$$

where $f_* = 1/2\pi L$ with $L = 1000$ km the arm length of the DECIGO detector [94]. This factor is actually the averaged detector response function, and it comes from the fact that the four constellations of three satellites of DECIGO are constantly orbiting around the sun, so the source orientation relative to each constellation plane varies over time. For our purpose of estimating the detection rate of memory signals, one can average it over the source orientation and the GW polarization angle. In the end, the factor $\sqrt{8}$ of Eq. (B5) arises from 8 uncorrelated interferometric signals, which are collected by the four independent constellations, having similar orbital configurations and sharing the same instrumental noise PSD [63, 95].

Appendix C: Simulation results based on a different population model

In the Main text, we presented the forecasted detection rates of memory signals using the binary black hole

(BBH) population model provided by Ref. [66] based on GWTC-3. Here, in this section, we used the models M33.A and M43.A in Ref. [77] to simulate the memories again. As one can find out, the detect rates are of the same orders of magnitude as those in the Main text.

As in the Main text, we still generated BBH systems with random right ascension (RA), declination (DEC), inclination angle ι , and coalescence phase ϕ . The stars run in quasi-circular orbits, with spins aligned to the orbital angular momentum. Their masses, spins, and merger rates were sampled from appropriate population synthesis models, influenced by factors such as common envelope physics, stellar remnant natal kicks, cosmic chemical evolution, and angular momentum transport during black hole formation [77]. The models, M33.A and M43.A, were employed here. Following Ref. [96], we combined the two models and sampled BBH systems, resulting in approximately 272,000 BBH merger events over DECIGO's 5-year operation. The distributions of chirp mass \mathcal{M} , mass ratio $q = m_1/m_2$, and redshift z are displayed in Fig. 6. As shown, most of the sampled BBH

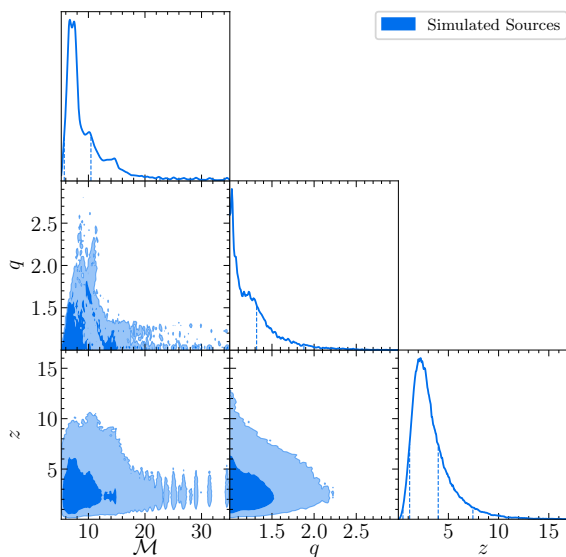


FIG. 6. The distributions of the source-frame chirp mass \mathcal{M} , mass ratio $q = m_1/m_2$, and redshift z , sampled from the combined M33.A and M43.A population synthesis models.

systems have small masses, with $\mathcal{M} \sim 8M_\odot$ and $q \sim 1$, while their redshifts range from 1 to 4. Using the sampled BBHs, we also used GWMemory to generate their memory waveforms, assuming the oscillatory parts last for 5×10^3 seconds.

Table II presents the numbers of detectable memory signals during DECIGO's 5-year observation period, meeting the SNR thresholds for different criteria. This table shows that up to 3,544 memory signals with SNRs

of at least 3 could be observed by DECIGO, higher than the number reported in the Main text. However, for higher SNR thresholds, the numbers here are smaller. This is due to the fact that there are fewer more massive

SNR Thresholds	10	8	5	3
Event Numbers	~ 33	~ 68	~ 392	~ 3544

TABLE II. The number of memory signals with sufficiently high SNRs that might be detected by DECIGO during its 5-year operation.

BBHs predicted by the population model used here.

Figure 7 shows the distributions of \mathcal{M} , q , and z for events with memory SNRs of at least 3 or 8. Again, a

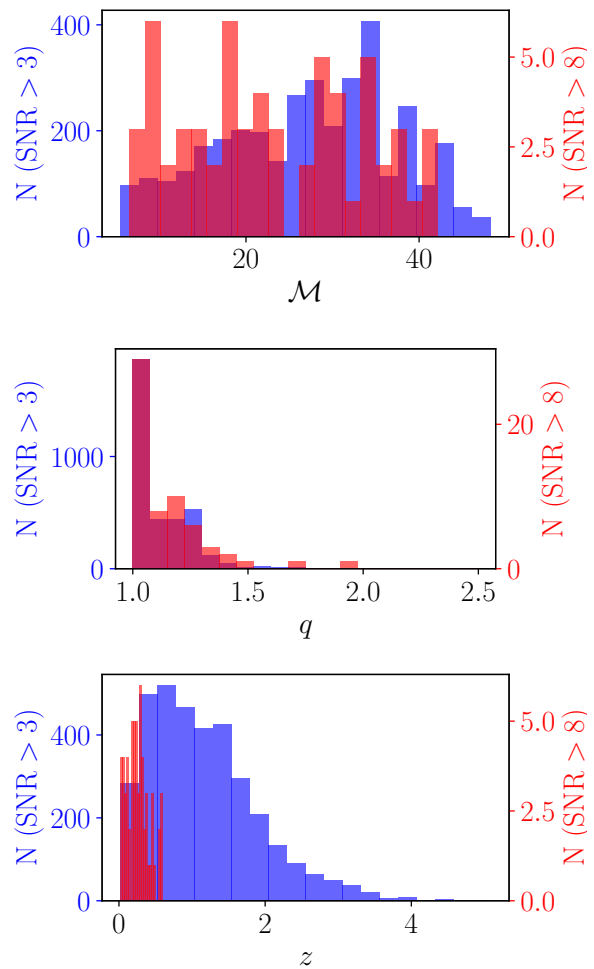


FIG. 7. The distributions of \mathcal{M} , q , and z for events with memory SNRs of at least 3 or 8. The left vertical axis corresponds to memory SNR > 3 , with a different scale from the right axis, which is for memory SNR > 8 .

large fraction of these systems have $q \sim 1$. The source redshift range does not change appreciably.

- [1] Y. B. Zel'dovich and A. G. Polnarev, Radiation of gravitational waves by a cluster of superdense stars, *Sov. Astron.* **18**, 17 (1974).
- [2] V. Braginsky and L. Grishchuk, Kinematic Resonance and Memory Effect in Free Mass Gravitational Antennas, *Sov. Phys. JETP* **62**, 427 (1985).
- [3] D. Christodoulou, Nonlinear nature of gravitation and gravitational-wave experiments, *Phys. Rev. Lett.* **67**, 1486 (1991).
- [4] K. S. Thorne, Gravitational-wave bursts with memory: The Christodoulou effect, *Phys. Rev. D* **45**, 520 (1992).
- [5] R. Sachs, Asymptotic symmetries in gravitational theory, *Phys. Rev.* **128**, 2851 (1962).
- [6] E. E. Flanagan and D. A. Nichols, Conserved charges of the extended Bondi-Metzner-Sachs algebra, *Phys. Rev. D* **95**, 044002 (2017), [arXiv:1510.03386 \[hep-th\]](#).
- [7] A. Strominger, [Lectures on the Infrared Structure of Gravity and Gauge Theory](#) (Princeton University Press, 2018) [arXiv:1703.05448](#).
- [8] A. Ashtekar, Radiative Degrees of Freedom of the Gravitational Field in Exact General Relativity, *J. Math. Phys.* **22**, 2885 (1981).
- [9] A. Strominger, On BMS invariance of gravitational scattering, *JHEP* **07**, 152, [arXiv:1312.2229 \[hep-th\]](#).
- [10] A. Strominger and A. Zhiboedov, Gravitational Memory, BMS Supertranslations and Soft Theorems, *JHEP* **01**, 086, [arXiv:1411.5745 \[hep-th\]](#).
- [11] S. Pasterski, A. Strominger, and A. Zhiboedov, New Gravitational Memories, *JHEP* **12**, 053, [arXiv:1502.06120 \[hep-th\]](#).
- [12] D. A. Nichols, Spin memory effect for compact binaries in the post-Newtonian approximation, *Phys. Rev. D* **95**, 084048 (2017), [arXiv:1702.03300 \[gr-qc\]](#).
- [13] D. A. Nichols, Center-of-mass angular momentum and memory effect in asymptotically flat spacetimes, *Phys. Rev. D* **98**, 064032 (2018), [arXiv:1807.08767 \[gr-qc\]](#).
- [14] G. Barnich and C. Troessaert, Symmetries of asymptotically flat 4 dimensional spacetimes at null infinity revisited, *Phys. Rev. Lett.* **105**, 111103 (2010), [arXiv:0909.2617 \[gr-qc\]](#).
- [15] G. Barnich and C. Troessaert, Aspects of the BMS/CFT correspondence, *JHEP* **05**, 062, [arXiv:1001.1541 \[hep-th\]](#).
- [16] M. Campiglia and A. Laddha, Asymptotic symmetries and subleading soft graviton theorem, *Phys. Rev. D* **90**, 124028 (2014), [arXiv:1408.2228 \[hep-th\]](#).
- [17] M. Campiglia and A. Laddha, New symmetries for the Gravitational S-matrix, *JHEP* **04**, 076, [arXiv:1502.02318 \[hep-th\]](#).
- [18] M. Campiglia and J. Peraza, Generalized BMS charge algebra, *Phys. Rev. D* **101**, 104039 (2020), [arXiv:2002.06691 \[gr-qc\]](#).
- [19] N. Khera, B. Krishnan, A. Ashtekar, and T. De Lorenzo, Inferring the gravitational wave memory for binary coalescence events, *Phys. Rev. D* **103**, 044012 (2021), [arXiv:2009.06351 \[gr-qc\]](#).
- [20] S. Tiwari, M. Ebersold, and E. Z. Hamilton, Leveraging gravitational-wave memory to distinguish neutron star-black hole binaries from black hole binaries, *Phys. Rev. D* **104**, 123024 (2021), [arXiv:2110.11171 \[gr-qc\]](#).
- [21] D. Lopez, S. Tiwari, and M. Ebersold, Gravitational wave memory of compact binary coalescence in the presence of matter effects, *Phys. Rev. D* **109**, 043039 (2024), [arXiv:2305.04761 \[gr-qc\]](#).
- [22] Y. Xu, M. Rosselló-Sastre, S. Tiwari, M. Ebersold, E. Z. Hamilton, C. García-Quirós, H. Estellés, and S. Husa, Enhancing gravitational wave parameter estimation with nonlinear memory: Breaking the distance-inclination degeneracy, *Phys. Rev. D* **109**, 123034 (2024), [arXiv:2403.00441 \[gr-qc\]](#).
- [23] B. Goncharov, L. Donnay, and J. Harms, Inferring Fundamental Spacetime Symmetries with Gravitational-Wave Memory: From LISA to the Einstein Telescope, *Phys. Rev. Lett.* **132**, 241401 (2024), [arXiv:2310.10718 \[gr-qc\]](#).
- [24] S. Hou and Z.-H. Zhu, Gravitational memory effects and Bondi-Metzner-Sachs symmetries in scalar-tensor theories, *JHEP* **01**, 083, [arXiv:2005.01310 \[gr-qc\]](#).
- [25] S. Tahura, D. A. Nichols, A. Saffer, L. C. Stein, and K. Yagi, Brans-Dicke theory in Bondi-Sachs form: Asymptotically flat solutions, asymptotic symmetries and gravitational-wave memory effects, *Phys. Rev. D* **103**, 104026 (2021), [arXiv:2007.13799 \[gr-qc\]](#).
- [26] A. Seraj, Gravitational breathing memory and dual symmetries, *JHEP* **05**, 283, [arXiv:2103.12185 \[hep-th\]](#).
- [27] S. Hou and Z.-H. Zhu, “Conserved charges” of the Bondi-Metzner-Sachs algebra in Brans-Dicke theory, *Chin. Phys. C* **45**, 023122 (2021), [arXiv:2008.05154 \[gr-qc\]](#).
- [28] S. Tahura, D. A. Nichols, and K. Yagi, Gravitational-wave memory effects in Brans-Dicke theory: Waveforms and effects in the post-Newtonian approximation, *Phys. Rev. D* **104**, 104010 (2021), [arXiv:2107.02208 \[gr-qc\]](#).
- [29] S. Hou, T. Zhu, and Z.-H. Zhu, Conserved charges in Chern-Simons modified theory and memory effects, *JCAP* **04** (04), 032, [arXiv:2112.13049 \[gr-qc\]](#).
- [30] L. Heisenberg, N. Yunes, and J. Zosso, Gravitational wave memory beyond general relativity, *Phys. Rev. D* **108**, 024010 (2023), [arXiv:2303.02021 \[gr-qc\]](#).
- [31] S. Hou, A. Wang, and Z.-H. Zhu, Asymptotic analysis of Einstein-Æther theory and its memory effects: The linearized case, *Phys. Rev. D* **109**, 044025 (2024), [arXiv:2309.01165 \[gr-qc\]](#).
- [32] S. Hollands and R. M. Wald, Conformal null infinity does not exist for radiating solutions in odd spacetime dimensions, *Class. Quant. Grav.* **21**, 5139 (2004), [arXiv:gr-qc/0407014](#).
- [33] S. Hollands, A. Ishibashi, and R. M. Wald, BMS Supertranslations and Memory in Four and Higher Dimensions, *Class. Quant. Grav.* **34**, 155005 (2017), [arXiv:1612.03290 \[gr-qc\]](#).
- [34] P. D. Lasky, E. Thrane, Y. Levin, J. Blackman, and Y. Chen, Detecting gravitational-wave memory with LIGO: implications of GW150914, *Phys. Rev. Lett.* **117**, 061102 (2016), [arXiv:1605.01415 \[astro-ph.HE\]](#).
- [35] H. Yang and D. Martynov, Testing Gravitational Memory Generation with Compact Binary Mergers, *Phys. Rev. Lett.* **121**, 071102 (2018), [arXiv:1803.02429 \[gr-qc\]](#).
- [36] M. Hübner, C. Talbot, P. D. Lasky, and E. Thrane, Measuring gravitational-wave memory in the first LIGO/Virgo gravitational-wave transient catalog, *Phys. Rev. D* **101**, 023011 (2020), [arXiv:1911.12496 \[astro-ph.HE\]](#).
- [37] Z.-C. Zhao, X. Liu, Z. Cao, and X. He, Gravitational wave memory of the binary black hole events in GWTC-

- 2, *Phys. Rev. D* **104**, 064056 (2021), [arXiv:2111.13882 \[gr-qc\]](#).
- [38] T. Islam, S. E. Field, G. Khanna, and N. Warburton, Survey of gravitational wave memory in intermediate mass ratio binaries, *Phys. Rev. D* **108**, 024046 (2023), [arXiv:2109.00754 \[gr-qc\]](#).
- [39] M. Hübner, P. Lasky, and E. Thrane, Memory remains undetected: Updates from the second LIGO/Virgo gravitational-wave transient catalog, *Phys. Rev. D* **104**, 023004 (2021), [arXiv:2105.02879 \[gr-qc\]](#).
- [40] S. Y. Cheung, P. D. Lasky, and E. Thrane, Does space-time have memories? Searching for gravitational-wave memory in the third LIGO-Virgo-KAGRA gravitational-wave transient catalogue, *Class. Quant. Grav.* **41**, 115010 (2024), [arXiv:2404.11919 \[gr-qc\]](#).
- [41] G. Agazie et al. (NANOGrav), The NANOGrav 12.5 yr Data Set: Search for Gravitational Wave Memory, *Astrophys. J.* **963**, 61 (2024), [arXiv:2307.13797 \[gr-qc\]](#).
- [42] A. M. Grant and D. A. Nichols, Outlook for detecting the gravitational-wave displacement and spin memory effects with current and future gravitational-wave detectors, *Phys. Rev. D* **107**, 064056 (2023), [Erratum: *Phys. Rev. D* **108**, 029901(E) (2023)], [arXiv:2210.16266 \[gr-qc\]](#).
- [43] S. Sun, C. Shi, J.-D. Zhang, and J. Mei, Detecting the gravitational wave memory effect with TianQin, *Phys. Rev. D* **107**, 044023 (2023), [arXiv:2207.13009 \[gr-qc\]](#).
- [44] S. Gasparotto, R. Vicente, D. Blas, A. C. Jenkins, and E. Barausse, Can gravitational-wave memory help constrain binary black-hole parameters? A LISA case study, *Phys. Rev. D* **107**, 124033 (2023), [arXiv:2301.13228 \[gr-qc\]](#).
- [45] H. Inchauspé, S. Gasparotto, D. Blas, L. Heisenberg, J. Zosso, and S. Tiwari, Measuring gravitational wave memory with LISA, [arXiv \(2024\)](#), [arXiv:2406.09228 \[gr-qc\]](#).
- [46] N. Seto, S. Kawamura, and T. Nakamura, Possibility of direct measurement of the acceleration of the universe using 0.1-Hz band laser interferometer gravitational wave antenna in space, *Phys. Rev. Lett.* **87**, 221103 (2001), [arXiv:astro-ph/0108011 \[astro-ph\]](#).
- [47] S. Kawamura et al., Space gravitational-wave antennas DECIGO and B-DECIGO, *Int. J. of Mod. Phys. D* **28**, 1845001 (2019).
- [48] S. Kawamura et al., Current status of space gravitational wave antenna DECIGO and B-DECIGO, *PTEP* **2021**, 05A105 (2021), [arXiv:2006.13545 \[gr-qc\]](#).
- [49] Indeed, the downscale version, B-DECIGO, was also expected to observe a lot of memory signals, qualitatively [97].
- [50] K. Mitman, J. Moxon, M. A. Scheel, S. A. Teukolsky, M. Boyle, N. Deppe, L. E. Kidder, and W. Thrope, Computation of displacement and spin gravitational memory in numerical relativity, *Phys. Rev. D* **102**, 104007 (2020), [arXiv:2007.11562 \[gr-qc\]](#).
- [51] H. Bondi, M. G. J. van der Burg, and A. W. K. Metzner, Gravitational waves in general relativity. 7. Waves from axisymmetric isolated systems, *Proc. Roy. Soc. Lond. A* **269**, 21 (1962).
- [52] R. K. Sachs, Gravitational waves in general relativity. 8. Waves in asymptotically flat space-times, *Proc. Roy. Soc. Lond. A* **270**, 103 (1962).
- [53] M. Favata, Post-Newtonian corrections to the gravitational-wave memory for quasi-circular, inspiralling compact binaries, *Phys. Rev. D* **80**, 024002 (2009), [arXiv:0812.0069 \[gr-qc\]](#).
- [54] M. Favata, Nonlinear gravitational-wave memory from binary black hole mergers, *Astrophys. J. Lett.* **696**, L159 (2009), [arXiv:0902.3660 \[astro-ph.SR\]](#).
- [55] M. Favata, The gravitational-wave memory effect, *Class. Quant. Grav.* **27**, 084036 (2010), [arXiv:1003.3486 \[gr-qc\]](#).
- [56] M. Favata, The Gravitational-wave memory from eccentric binaries, *Phys. Rev. D* **84**, 124013 (2011), [arXiv:1108.3121 \[gr-qc\]](#).
- [57] C. Talbot, E. Thrane, P. D. Lasky, and F. Lin, Gravitational-wave memory: waveforms and phenomenology, *Phys. Rev. D* **98**, 064031 (2018), [arXiv:1807.00990 \[astro-ph.HE\]](#).
- [58] S. Husa, S. Khan, M. Hannam, M. Pürrer, F. Ohme, X. Jiménez Forteza, and A. Bohé, Frequency-domain gravitational waves from nonprecessing black-hole binaries. I. New numerical waveforms and anatomy of the signal, *Phys. Rev. D* **93**, 044006 (2016), [arXiv:1508.07250 \[gr-qc\]](#).
- [59] S. Khan, S. Husa, M. Hannam, F. Ohme, M. Pürrer, X. Jiménez Forteza, and A. Bohé, Frequency-domain gravitational waves from nonprecessing black-hole binaries. II. A phenomenological model for the advanced detector era, *Phys. Rev. D* **93**, 044007 (2016), [arXiv:1508.07253 \[gr-qc\]](#).
- [60] G. Nelemans, L. R. Yungelson, and S. F. Portegies Zwart, The gravitational wave signal from the galactic disk population of binaries containing two compact objects, *Astron. Astrophys.* **375**, 890 (2001), [arXiv:astro-ph/0105221](#).
- [61] A. J. Farmer and E. S. Phinney, The gravitational wave background from cosmological compact binaries, *Mon. Not. Roy. Astron. Soc.* **346**, 1197 (2003), [arXiv:astro-ph/0304393](#).
- [62] K. Yagi and T. Tanaka, DECIGO/BBO as a probe to constrain alternative theories of gravity, *Prog. Theor. Phys.* **123**, 1069 (2010), [arXiv:0908.3283 \[gr-qc\]](#).
- [63] S. Kawamura et al., The Japanese space gravitational wave antenna: DECIGO, Laser interferometer space antenna. Proceedings, 8th International L
- [64] K. Yagi and N. Seto, Detector configuration of DECIGO/BBO and identification of cosmological neutron-star binaries, *Phys. Rev. D* **83**, 044011 (2011), [Erratum: *Phys. Rev. D* **95**, 109901(E) (2017)], [arXiv:1101.3940 \[astro-ph.CO\]](#).
- [65] M. Sun, J. Li, S. Cao, and X. Liu, Deep learning forecasts of cosmic acceleration parameters from DECIGO-hertz Interferometer Gravitational-wave Observatory, *Astron. Astrophys.* **682**, A177 (2024), [arXiv:2307.16437 \[astro-ph.GA\]](#).
- [66] R. Abbott et al. (KAGRA, VIRGO, LIGO Scientific), Population of Merging Compact Binaries Inferred Using Gravitational Waves through GWTC-3, *Phys. Rev. X* **13**, 011048 (2023), [arXiv:2111.03634 \[astro-ph.HE\]](#).
- [67] P. Madau and M. Dickinson, Cosmic Star Formation History, *Ann. Rev. Astron. Astrophys.* **52**, 415 (2014), [arXiv:1403.0007 \[astro-ph.CO\]](#).
- [68] GWMemory was used to accelerate the simulation.
- [69] S. Isoyama, H. Nakano, and T. Nakamura, Multiband Gravitational-Wave Astronomy: Observing binary inspirals with a decihertz detector, B-DECIGO, *PTEP* **2018**, 073E01 (2018), [arXiv:1802.06977 \[gr-qc\]](#).
- [70] D. Gerosa, S. Ma, K. W. K. Wong, E. Berti,

- R. O’Shaughnessy, Y. Chen, and K. Belczynski, Multi-band gravitational-wave event rates and stellar physics, *Phys. Rev. D* **99**, 103004 (2019), arXiv:1902.00021 [astro-ph.HE].
- [71] S. E. Timpano, L. J. Rubbo, and N. J. Cornish, Characterizing the galactic gravitational wave background with LISA, *Phys. Rev. D* **73**, 122001 (2006), arXiv:gr-qc/0504071.
- [72] M. L. Katz and S. L. Larson, Evaluating Black Hole Detectability with LISA, *Mon. Not. Roy. Astron. Soc.* **483**, 3108 (2019), arXiv:1807.02511 [gr-qc].
- [73] E. Gourgoulhon, A. Le Tiec, F. H. Vincent, and N. Warburton, Gravitational waves from bodies orbiting the Galactic Center black hole and their detectability by LISA, *Astron. Astrophys.* **627**, A92 (2019), arXiv:1903.02049 [gr-qc].
- [74] S. Babak, C. Caprini, D. G. Figueroa, N. Karnesis, P. Marcoccia, G. Nardini, M. Pieroni, A. Ricciardone, A. Sesana, and J. Torrado, Stochastic gravitational wave background from stellar origin binary black holes in LISA, *JCAP* **08**, 034, arXiv:2304.06368 [astro-ph.CO].
- [75] A. D. Johnson, S. J. Kapadia, A. Osborne, A. Hixon, and D. Kennefick, Prospects of detecting the nonlinear gravitational wave memory, *Phys. Rev. D* **99**, 044045 (2019), arXiv:1810.09563 [gr-qc].
- [76] To estimate the SNR for the inspiral stage, we used IMRPhenomD to generate the frequency-domain oscillatory waveform up to the frequency $f_{\max} = 0.018/(m_1 + m_2)$ [59], which was substituted into the frequency-domain memory waveform (3).
- [77] K. Belczynski et al., Evolutionary roads leading to low effective spins, high black hole masses, and O1/O2 rates for LIGO/Virgo binary black holes, *Astron. Astrophys.* **636**, A104 (2020), arXiv:1706.07053 [astro-ph.HE].
- [78] C. L. Rodriguez, P. Amaro-Seoane, S. Chatterjee, K. Kremer, F. A. Rasio, J. Samsing, C. S. Ye, and M. Zevin, Post-Newtonian Dynamics in Dense Star Clusters: Formation, Masses, and Merger Rates of Highly-Eccentric Black Hole Binaries, *Phys. Rev. D* **98**, 123005 (2018), arXiv:1811.04926 [astro-ph.HE].
- [79] Z. Cao and W.-B. Han, Waveform model for an eccentric binary black hole based on the effective-one-body-numerical-relativity formalism, *Phys. Rev. D* **96**, 044028 (2017), arXiv:1708.00166 [gr-qc].
- [80] X. Liu, Z. Cao, and Z.-H. Zhu, A higher-multipole gravitational waveform model for an eccentric binary black holes based on the effective-one-body-numerical-relativity formalism, *Class. Quant. Grav.* **39**, 035009 (2022), arXiv:2102.08614 [gr-qc].
- [81] M. Milosavljevic and D. Merritt, The Final parsec problem, *AIP Conf. Proc.* **686**, 201 (2003), arXiv:astro-ph/0212270.
- [82] V. B. Braginskii and K. S. Thorne, Gravitational-wave bursts with memory and experimental prospects, *Nature* **327**, 123 (1987).
- [83] T. Yang, R.-G. Cai, Z. Cao, and H. M. Lee, Eccentricity of Long Inspiring Compact Binaries Sheds Light on Dark Sirens, *Phys. Rev. Lett.* **129**, 191102 (2022), arXiv:2202.08608 [gr-qc].
- [84] R. N. Lang, Compact binary systems in scalar-tensor gravity. II. Tensor gravitational waves to second post-Newtonian order, *Phys. Rev. D* **89**, 084014 (2014), arXiv:1310.3320 [gr-qc].
- [85] R. N. Lang, Compact binary systems in scalar-tensor gravity. III. Scalar waves and energy flux, *Phys. Rev. D* **91**, 084027 (2015), arXiv:1411.3073 [gr-qc].
- [86] S. Hou, T. Zhu, and Z.-H. Zhu, Asymptotic analysis of Chern-Simons modified gravity and its memory effects, *Phys. Rev. D* **105**, 024025 (2022), arXiv:2109.04238 [gr-qc].
- [87] K. Chamberlain and N. Yunes, Theoretical Physics Implications of Gravitational Wave Observation with Future Detectors, *Phys. Rev. D* **96**, 084039 (2017), arXiv:1704.08268 [gr-qc].
- [88] L. Heisenberg, G. Xu, and J. Zosso, Unifying ordinary and null memory, *JCAP* **05**, 119, arXiv:2401.05936 [gr-qc].
- [89] R. M. Wald, *General Relativity* (University of Chicago Press, Chicago, IL, 1984).
- [90] L. Bieri and D. Garfinkle, Perturbative and gauge invariant treatment of gravitational wave memory, *Phys. Rev. D* **89**, 084039 (2014), arXiv:1312.6871 [gr-qc].
- [91] G. Pratten et al., Computationally efficient models for the dominant and subdominant harmonic modes of precessing binary black holes, *Phys. Rev. D* **103**, 104056 (2021), arXiv:2004.06503 [gr-qc].
- [92] J. N. Goldberg, A. J. MacFarlane, E. T. Newman, F. Rohrlich, and E. C. G. Sudarshan, Spin s spherical harmonics and edth, *J. Math. Phys.* **8**, 2155 (1967).
- [93] C. Zhang, Q. Gao, Y. Gong, B. Wang, A. J. Weinstein, and C. Zhang, Full analytical formulas for frequency response of space-based gravitational wave detectors, *Phys. Rev. D* **101**, 124027 (2020), arXiv:2003.01441 [gr-qc].
- [94] S. Kawamura et al., The Japanese space gravitational wave antenna DECIGO, *Class. Quant. Grav.* **23**, S125 (2006).
- [95] A. Balcerzak and M. P. Dabrowski, Redshift drift in a pressure gradient cosmology, *Phys. Rev. D* **87**, 063506 (2013), arXiv:1210.6331 [astro-ph.CO].
- [96] J.-P. Zhu, S. Wu, Y.-P. Yang, B. Zhang, Y.-W. Yu, H. Gao, Z. Cao, and L.-D. Liu, No Detectable Kilonova Counterpart is Expected for O3 Neutron Star–Black Hole Candidates, *Astrophys. J.* **921**, 156 (2021), arXiv:2106.15781 [astro-ph.HE].
- [97] M. Ando, Possibility of Observation of Gravitational-Wave Memory Effect by B-DECIGO, https://www.dropbox.com/scl/fi/v3g05k1teex8379yd0jyg/rinko230203_ando.pdf?rlkey=27j7ib1sy1ycmac36k70mk6qw&dl=0 (2022), KMI Inter-Region Seminar, Nagoya university.